

Temperature dependence of instantons in QCD

M.-C. Chu,¹ S. M. Ouellette,² S. Schramm,³ and R. Seki^{4,5}

¹*Department of Physics and the Institute of Mathematical Sciences, The Chinese University of Hong Kong, Shatin, N.T., Hong Kong*

²*Lauritsen Laboratory, Caltech 452-48, Pasadena, California 91125*

³*GSI, Darmstadt, Germany*

⁴*W. K. Kellogg Radiation Laboratory, Caltech 106-38, Pasadena, California 91125*

⁵*Department of Physics California State University, Northridge, California 91330*

(Received 15 June 1999; published 12 October 2000)

We investigate the temperature dependence of the instanton content of gluon fields, using unquenched lattice QCD and the cooling method. The topological susceptibility arising from instantons decreases rapidly below the phase-transition temperature T_c (≈ 150 MeV), becoming practically zero at $T \approx T_c$. The dominant calorons size parameter deduced from the correlation function decreases from about 0.9 fm below T_c to 0.4 fm at $1.3T_c$. The instanton charge distribution is Poissonian above T_c with deviations at low temperature.

PACS number(s): 12.38.Gc, 11.10.Wx, 12.38.Mh

I. INTRODUCTION

Among the four global symmetries associated with quantum chromodynamics (QCD), two chiral symmetries $SU(N_f)_A$ and $U(1)_A$ must be broken as the observed hadron spectrum suggests. At high temperature it is expected that the two symmetries are restored. The question as to how they are restored is an important issue, especially in relation to the QCD deconfinement phase transition (or maybe a crossover), and is recently attracting much attention [1–5]. The phase transition from deconfinement to the confining regime is thought to have occurred in the evolution of the early universe. Inversely, heating up ordinary matter beyond the critical temperature is expected to generate a new phase of matter, the quark-gluon plasma (QGP), which is under investigation in ultrarelativistic heavy-ion collisions.

Instantons, i.e., tunneling events between topologically different gauge vacua, are believed to play a crucial role in the breaking and restoration of the chiral symmetries, and perhaps also in the deconfinement phase transition [2]: The $SU(N_f)_A$ symmetry manifests itself in the Goldstone mode through chiral condensates generated dynamically by instantons. A similar mechanism may be at work in the formation of hadronic bound states, and the $SU(N_f)_A$ restoration and the deconfinement are thus closely related to each other. The $U(1)_A$ symmetry is spontaneously broken by the chiral anomaly driven by instantons. At high temperatures, the restoration of the symmetries takes place because instanton amplitudes are suppressed through Debye screening, which induces the gluons to be (electrically) massive.

How realistic is this instanton mechanism, and what is the precise dynamics of the instanton participation? The best means to answer the questions is the lattice gauge theory [6], which provides a systematic, nonperturbative framework to study the equilibrium properties of QCD at both zero and finite temperatures. Whereas direct comparison between lattice results and experiments is not always possible, lattice QCD often motivates and constrains phenomenological models, which connect QCD with experiments. Here, the use of *unquenched* QCD is essential, since the instanton mechanism

is expected to be affected by the presence of the dynamical quarks.

In this paper, we report unquenched lattice QCD results on the temperature dependence of the instanton contents of gluons. The calculation is carried out for $16^3 \times N_t$ lattices with $N_t=4, 6, 8, 10, 12, 14,$ and 16 for quark masses $m_q a = 0.0125$ and two flavors. The temperature is varied by changing N_t , with $\beta=5.54$ fixed. The topological susceptibility and the topological charge correlation are observed to be stable with respect to the number of cooling steps.

In Sec. II, we discuss the observables we calculate with unquenched lattice QCD, and describe in Sec. III how we generate and cool gauge configurations. Our results are presented in Sec. IV, and conclusions and discussions are given in Sec. V.

II. OBSERVABLES

The instanton content of the gauge fields is monitored by the topological-charge density, which can be measured on the lattice with

$$Q(x_n) = -\frac{1}{32\pi^2} \epsilon_{\alpha\beta\gamma\delta} \text{Re Tr}[U_{\alpha\beta}(x_n)U_{\gamma\delta}(x_n)], \quad (1)$$

where $U_{\alpha\beta}$ is the product of the link variables around a plaquette in the α - β plane. A direct calculation of Q from gauge configurations is plagued with poor statistics and with lattice artifacts associated with discretization. Teper *et al.* [7] have shown that the quenched topological charge can be reliably extracted using the cooling method, in which one applies a certain number of smoothing steps to each configuration in order to minimize the action locally. The ultraviolet fluctuations are quickly suppressed by these cooling steps, and only the relatively stable instantons are left in the configuration, making it easy to extract the topological charge. However, as one cools a configuration, annihilation of nearby instanton-antiinstanton pairs could be induced, resulting in potential systematic errors in some topological observables. Improved methods have been developed recently to remedy the situation, such as cooling with an improved ac-

tion so as to forbid the decay of larger instantons [5] and the cycling method [8]. Details of the cooling method are discussed in Refs. [7,9].

The topological susceptibility is then given as the fluctuations of the topological charge:

$$\chi_t \equiv \frac{1}{N_t N_s^3 a^4} \left\langle \left(\sum_n Q(x_n) \right)^2 \right\rangle, \quad (2)$$

where angle brackets indicate configuration averaging, N_t and N_s are the number of sites in the temporal and spatial direction, respectively, and a is the lattice spacing.

In order to examine the details of the topological-charge distribution, we also calculate the topological charge-density correlation function [9]

$$C_Q(x) = \frac{\left\langle \sum_y Q(y) Q(x+y) \right\rangle}{\left\langle \sum_{y_h} Q^2(y) \right\rangle}. \quad (3)$$

One can compare this correlation function to a convolution of an isolated instanton topological-charge density

$$Q_\rho(x) = \frac{6}{\pi^2 \rho^4} \left(\frac{\rho^2}{x^2 + \rho^2} \right)^4. \quad (4)$$

Zero-temperature calculations using the cooling method [9] show that after about 50 cooling steps, the gauge fields are dominated by large, isolated instantons, whose profiles agree well with Eq. (4).

III. GAUGE CONFIGURATIONS AND COOLING

To generate the unquenched gauge configurations, we adopted and modified a code written by the MILC Collaboration [10], using dynamical staggered fermions. Forty configurations are generated for each of $N_t=14$ and 16, and 100, 80, 76, 73, and 89 configurations for $N_t=4, 6, 8, 10$, and 12, respectively. In each case, a molecular-dynamics time step of $dt=0.02$ is used, and the first 300 time units (43 for $N_t=14$, 16) from a hot start are used as thermalization. The configurations were separated by 3 time units for $N_t=14$ and 16, 50 time units for $N_t=4, 6, 8, 10$, and 12.

As is well known, topological quantities are correlated over a long molecular-dynamics time in configurations generated with the hybrid molecular dynamics method [11,12]. Recent results indicate that the problem may be less serious for Wilson fermions than Kogut-Susskind fermions [13,14]. For Kogut-Susskind fermions, the problem of decorrelating the topological charge becomes especially serious near the chiral limit, and it was found that the autocorrelation time grows to above 200 time units for $\beta=5.35$ and $ma=0.010$ [12]. We find that for our set of parameters, 50 time units are necessary to decorrelate the configurations. We show a history of the topological charges for $N_t=10$ in Fig. 1. Each data point denoted by the open circles represents the topological charge Q in a configuration. It is clear from the figure that the topological charges extracted from most configurations are closed to (typically within 10% of) integers, as indicated by the dashed lines. Taking 300 time units for ther-

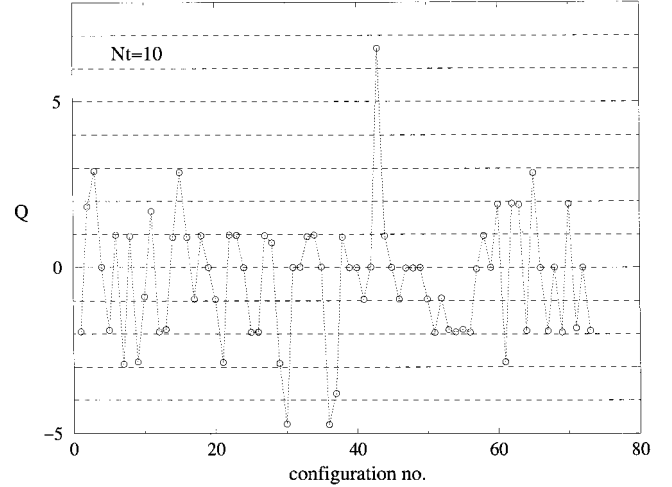


FIG. 1. Topological charges in the $N_t=10$ configurations, where 300 molecular dynamics time units were discarded in the beginning for thermalization, and consecutive configurations are separated by 50 time units. The dotted line is drawn to guide the eyes.

malization and 50 time units for the separation between configurations seems to be adequate, and there are no visible correlation or thermalization effects. However, this means a total of over 5000 time units for each N_t , and it becomes very expensive for $N_t=14$ and 16. Being limited in computing resources, we settle with shorter runs for $N_t=14$ and 16. The correlations in our $N_t=14$ and 16 configurations are probably quite large, and the error bars for those results are therefore underestimated; with this caveat in mind we nevertheless show them together with those of smaller N_t for comparison.

These configurations are then cooled, using the standard procedure as used in Ref. [9], for 200 steps, saving the fields every 20 steps. In quenched calculations, topological quantities such as those we discuss here are very stable with respect to cooling; measuring the topological charge density or their correlations at 50 or 100 cooling steps give the same results within the error bars. We have monitored our observables with respect to cooling for the unquenched calculation, and we have observed similar stability. For example, we show in Fig. 2 the topological-charge density correlation for $N_t=10$ at 100th, 160th, and 200th steps. The results coincide within the error bars. The topological susceptibility is slightly more sensitive to cooling, but it also settles to a stable value by 100 cooling steps. The results reported here are based on those extracted after 200 cooling steps.

The temperature of the system is given by $T=1/(N_t a)$ and can be varied by changing either N_t or a . The lattice spacing a is a function of the lattice inverse coupling β and can be calculated by perturbation theory for a narrow range of β in the asymptotic scaling regime. In order to obtain the temperature dependence reliably, we choose to vary the temperature by varying N_t , keeping a and β (and therefore also the quark mass ma) fixed. In this way, the uncertainty in a enters only as an overall constant factor, which does not affect the functional relationship between $\chi_t T$ significantly.

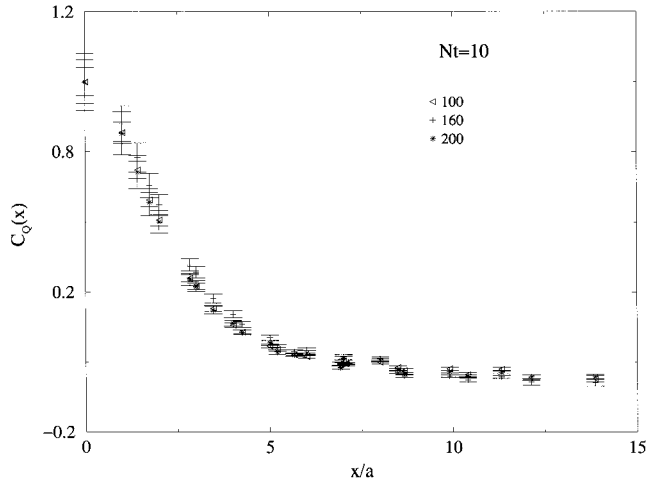


FIG. 2. Topological-charge density correlation function $C_Q(x)$ for $N_t=10$ at 100th, 160th, and 200th cooling steps. Results coincide within the statistical error bars.

The price we pay is that the calculation can be done only for a limited number of temperatures corresponding to the discrete values of N_t . This is especially problematic at high temperatures. The phase transition with the parameters we use occurs at $N_t=8$ and a temperature of $T_c=150(9)$ MeV [10], giving $a\approx 0.17$ fm.

IV. RESULTS

A. Topological susceptibility and charge correlation

The topological susceptibility χ_t is shown in Fig. 3 as a function of the temperature. In the quenched theory, the topological susceptibility is proportional to the instanton density [7]. Indeed, it was shown in Ref. [15] that two model calculations of the temperature dependence of the instanton density gave reasonably good description of the quenched topological susceptibility. At low temperature, the PCAC (partial conservation of axial vector current) suppression due to soft pion gas [16] agrees well with the quenched results, and at high temperature, the topological susceptibility follows the same trend as the Debye-screening suppression of instantons [17]. The unquenched topological susceptibility is not directly related to the instanton density. We nevertheless show the results of these model calculations in Fig. 3 as a comparison. The dashed curve in the figure is the PCAC suppression of the instanton density that is believed to be relevant for low temperature $T\ll T_c$ [16]:

$$\chi_t(T) = \chi_t(T=0)(1 + cT^2/F_\pi^2). \quad (5)$$

Equation (5) does not fit the rapid suppression of the topological susceptibility around T_c , even with $c=-0.36$, a value that is well outside the allowed range based on the PCAC argument $-1/6\leq c\leq 1/6$ [16]. Also shown in Fig. 3 is the perturbative Debye-screening prediction (for $N_c=3$, $N_f=2$) [17]:

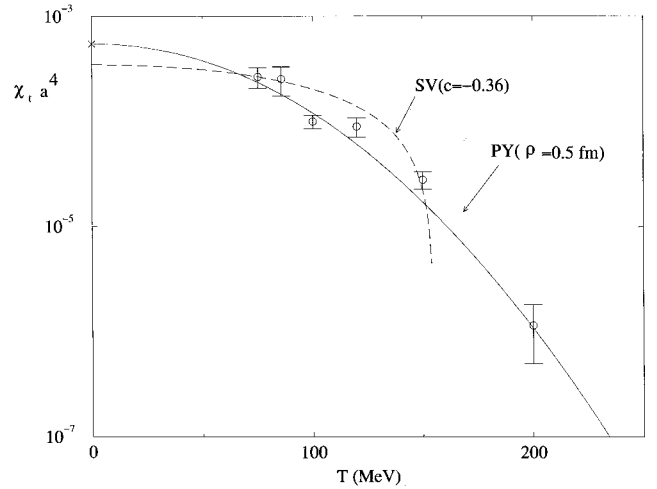


FIG. 3. Topological susceptibility as a function of temperature. The data points correspond to our unquenched-QCD-plus-cooling results with $N_t=6, 8, 10, 12, 14, 16$, and $a=0.17$ fm is assumed. The phase transition temperature T_c is approximately 150 MeV for our calculations with $\beta=5.54$, $ma=0.0125$, $N_x=16$. The dashed curve is the prediction of a PCAC model, Eq. (6), with $c=-0.36$, and the solid curve is that of a Debye-screening model, Eq. (7), with the instanton size parameter, $\rho=0.5$ fm.

$$\chi_t(t) = \chi_t(T=0)(1 + \lambda^2/3)^{7/6} \times \exp[-8\lambda^2/3 - 14\alpha(1 + \gamma\lambda^{-3/2})^{-8}], \quad (6)$$

where $\lambda \equiv \pi\rho T$, $\alpha=0.01289764$, and $\lambda=0.15858$. The solid curve corresponds to $\rho=0.5$ fm, arbitrarily normalized to the quenched value of the zero-temperature susceptibility [4] $\chi_t(T=0)=(180 \text{ MeV})^4$, which also agrees with phenomenology [18]. Equation (6) is not expected to be valid below T_c , but should become relevant at high temperatures. We observe that the curve for $\rho=0.5$ fm fits the data surprisingly well. This observation suggests that the Debye-screening mechanism may already be operative for $T<T_c$. Our $N_t=4$ ($T=2T_c$) result is not reliable because of severe finite-size effects and because not a single instanton is found in our 100 configurations. Also, our method of temperature variation by varying N_t provides only sparse data in the high-temperature regime.

The general features of the temperature dependence of χ_t are the same in the quenched calculation [15] and in the present unquenched calculation, but detailed features differ significantly. The unquenched χ_t decreases more slowly at low temperature, but goes down much more rapidly around T_c . The χ_t is suppressed by almost 90% at $T=T_c$ in the unquenched case, while it is only 50% in the quenched case. That is, the suppression of the instanton amplitudes is *enhanced* by the dynamical quarks. The rapid decrease in χ_t continues above T_c , so that only about 1% remains at $1.3 T_c$, compared to about 10% in the quenched calculation.

We show in Fig. 4 the topological charge correlation functions in comparison with the profile of an isolated instanton, Eq. (4), at $N_t=10$ ($T=120$ MeV) and $N_t=6$ ($T=200$ MeV). The symmetry of the data with respect to the

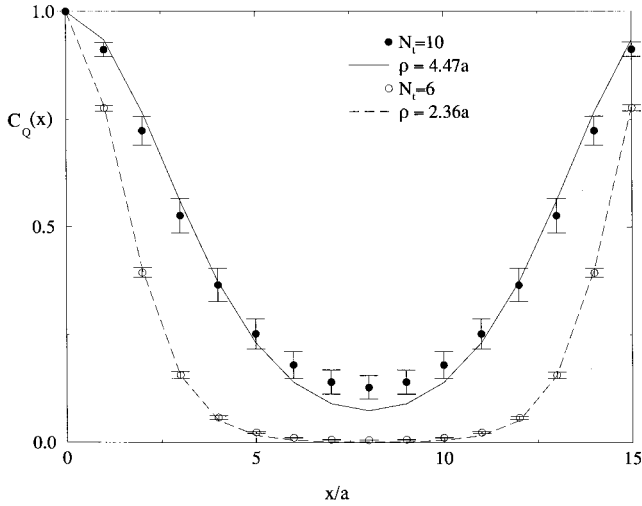


FIG. 4. Topological charge correlation function below ($N_t = 10$, $T = 120$ MeV) and above the phase transition ($N_t = 6$, $T = 200$ MeV). The lines are calculated by folding the profile of an isolated instanton, which when compared with the lattice data, give the values of the dominant caloron size parameter. They are $\bar{\rho} \approx 0.76$ fm (solid line) and 0.4 fm (dashed line) at $T = 120$ and 200 MeV, respectively.

mid-point of the lattice is a result of the periodic boundary condition. In the quenched calculations, $C_Q(r)$ is practically independent of the temperature, following remarkably closely to the profile, though hints of a transition to a smaller size parameter have been observed above T_c [15]. The present unquenched calculation clearly shows a rapid transition to a smaller size around T_c .

B. Caloron size and distribution

At finite temperatures, an instanton is deformed into a caloron, the core of which has a profile identical to a zero-temperature instanton with a renormalized size parameter [19]

$$\rho^2 = \rho_{T=0}^2 / (1 + \lambda^2/3), \quad (7)$$

which is valid at low temperature and $\lambda \equiv \pi\rho T$. The values of the caloron size-parameter ρ are extracted from the topological charge distribution using several methods. First we determine the positions of the instantons on the lattice by searching for the maxima (and minima) $|Q|_{\max}$ of the topological charge distribution and then fitting the shape of an instanton around the peak to the analytical form Eq. (4). In practice, we average the values of the topological charge around the peak in all spatial directions, which introduces some uncertainties because of discretization effects. We then use 3 or 5 points of the averaged radial shape of the instanton close to its maximum to fit the numerical data (Fig. 4 shows the result from the three-point fit). The number of points used for the fitting does not affect the resulting values for the radius parameter significantly. Secondly, one can convert

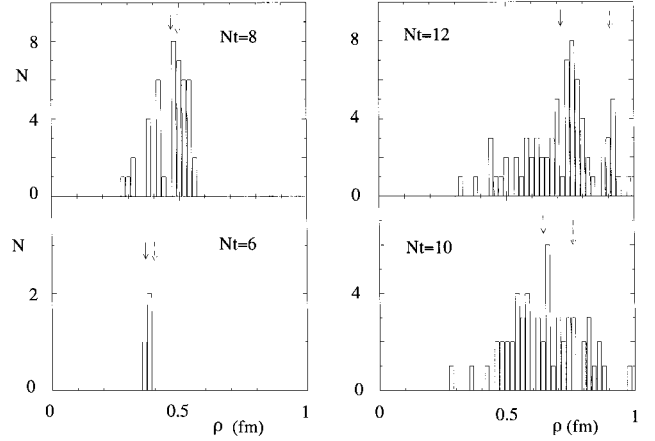


FIG. 5. Distribution of caloron size parameters for $N_t = 6, 8, 10$, and 12 . The arrows indicate the mean ($\bar{\rho}$, solid lines) and the dominant ($\tilde{\rho}$, dashed lines) size parameters.

the heights of the peaks to the sizes of the instantons by using Eq. (4), once the peak locations ($x = 0$) are identified:

$$\rho = \left(\frac{6}{\pi^2 |Q|_{\max}} \right)^{1/4}. \quad (8)$$

Finally, a direct fitting of the correlation functions to the convolution of an isolated instanton also gives an estimate for ρ . We have used all these methods, and they yield results that agree with each other within the error bars. We emphasize that the extraction of instanton/caloron size parameters is in general ansatz dependent, and the results we present here are valid only for isolated instantons/calorons. Note that for high temperatures and/or large calorons, when the deformation of instanton is large, the isotropic fit used here introduces a systematic error. However, the fact that fits to the peak value of the charge and to the slope of the correlation function agree with each other within statistics is a sign that the anisotropy is not problematic in the regime we study, where most calorons are small compared to our lattices and the topological charge density is dominated by the caloron core region.

The final value of the caloron size parameter can be then determined in two different ways, either by averaging a set of the parameter values fit to individual configurations, or by fitting to the configuration-averaged topological-charge density correlation functions. The parameter determined in the former way is the *mean* caloron size $\bar{\rho}$, and the parameter in the latter way is the *dominant* caloron size $\tilde{\rho}$. The two parameter values are in general different, but are close in our case as shown later in Fig. 5.

In Fig. 4, we show the temperature dependence of the caloron size parameter only around T_c for clarity. The dominant size parameter, $\tilde{\rho}$, shown in the figure is obtained by folding the profile of an isolated instanton. $\tilde{\rho}$ is approximately 0.76 fm at $0.8 T_c$, shrinks rapidly around T_c , and becomes about 0.4 fm at $1.3 T_c$.

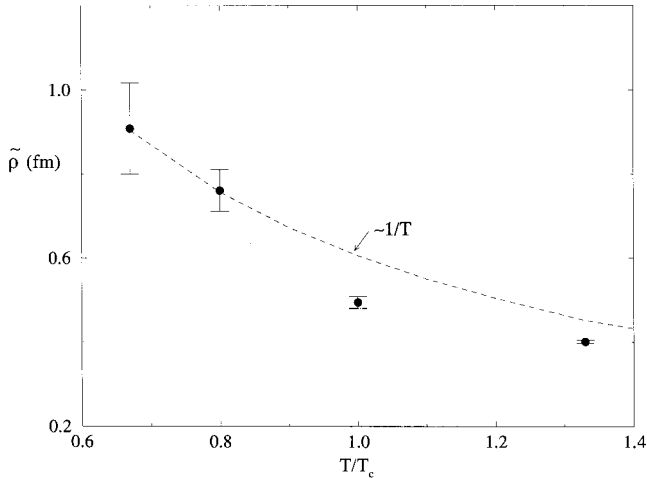


FIG. 6. Dominant caloron size parameter $\tilde{\rho}$ versus temperature, showing a clear fall-off around T_c .

To study closely the transition in the caloron size parameter, we calculate ρ for *each* configuration at $N_t=6, 8, 10,$ and 12 and plot the distribution of ρ in Fig. 5. Note that because of the suppression of the instantons above T_c , there are much less instantons at $N_t=6$, making it difficult to find the mean instanton size. Nevertheless, there is a clear trend that the means $\bar{\rho}$, marked by solid arrows in Fig. 5, as well as the widths of the ρ -distribution *decrease* as temperature goes up. In Fig. 5, we also show the dominant caloron size $\tilde{\rho}$ by the dashed arrows.

We show in Fig. 6 the dominant caloron size parameter $\tilde{\rho}$ as a function of temperature. At low temperature, $\tilde{\rho}$ turns out to be distinctly larger than the dilute-gas model prediction or the quenched results [15]. Its value at high temperature agrees roughly with that of the instanton liquid model [2]. Also shown in the figure is a $1/T$ dependence for comparison (dashed line). Note that we plot $\tilde{\rho}$ and not $\tilde{\rho}_{T=0}$ via Eq. (7) in Fig. 6, and this temperature dependence of the caloron size

parameter is not due to the simple renormalization in Eq. (7). In fact, if we had try to remove the effect of the simple renormalization according to Eq. (7), the temperature dependence of the instanton size parameter would be even *stronger*, due to the fact that the small caloron sizes at high temperatures *reduce* the effect of temperature renormalization, such that λ is *greater* at $T=0.8T_c$ than at $T=1.33T_c$. Several notes of cautions are in order. First, the rather small error bar for the size parameter at the highest temperature originates from the fact that the numbers are dominated by only three configurations with similarly-sized instantons. Second, the largest instantons are of size comparable to the lattice and therefore probably suffer large finite-size distortions.

The distribution of instanton charges in our configurations is shown as histograms for each N_t in Fig. 7. Whereas in the quenched case, these distributions agree with the convoluted Poisson distribution [15], the unquenched results show significant deviations from it. Our data suggests that the dynamical quarks have induced nontrivial correlations among the instantons at low temperatures. Above the phase transition, the distributions become Poissonian, suggesting a return to the dilute-gas ensemble. We caution the readers that the deviations from Poisson distribution at low temperature as suggested by our data could be an artifact of insufficient statistics, and more extensive study of the issue is called for.

V. SUMMARY AND DISCUSSIONS

Our key results are summarized as follows. We find that the topological susceptibility decreases slowly at low temperatures as the temperature increases, but a rapid suppression sets in around the phase transition temperature $T_c \approx 150$ MeV, so that, compared to the value at $T=0$, it is already down by an order of magnitude at T_c and becomes only

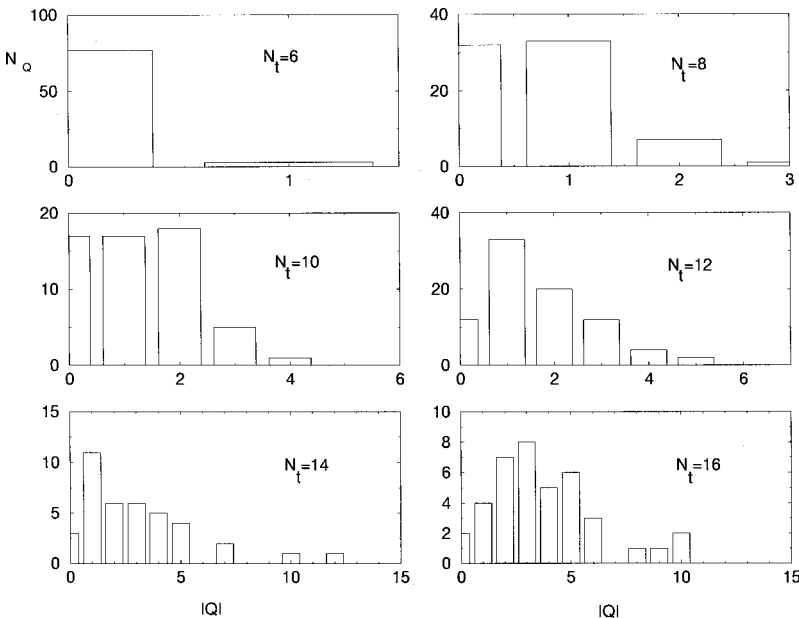


FIG. 7. Histograms showing the distribution of topological charges in the configurations for $N_t=6, 8, 10, 12,$ and 16 . $|Q|$ is the magnitude of the topological charges in a configuration, and $N(Q)$ is the frequency.

about 1% at $1.3 T_c$. This temperature dependence of the topological susceptibility is consistent with the Debye-screening model, using a caloron size parameter that agrees roughly with our own data. Accompanying this rapid change in χ_t is a transition of the dominant caloron size from about 0.9 fm at low temperature to 0.4 fm at $1.3 T_c$. Because of the cooling method we used, we observe neither small instantons nor instanton molecules, although we looked (unsuccessfully) for signs of molecules in the early cooling states where they might not have been annihilated. We also find curious temperature dependence of the instanton charge distribution; its deviations from Poissonian at low temperature might be related to nontrivial correlations among the instantons, which are suppressed above the phase transition. The nature and the details of this potential correlation are yet unclear, however, as is whether it corresponds to any of the dynamical models [2]. However, our data can only be considered suggestive, owing to its limited statistics, and a more extensive study of this issue is called for.

ACKNOWLEDGMENTS

This work is in part based on the MILC Collaboration's public lattice gauge theory code. We thank C. DeTar and C. McNeile for their technical assistance. We acknowledge the use of T3E's of National Partnership for Advanced Computational Infrastructure (NPACI) at the San Diego Supercomputer Center and at the Texas Advanced Computing Center and also of T3E's at the National Energy Research Scientific Computing Center (NERSC). This research was partially supported by the U.S. National Science Foundation under Grants No. PHY94-12818 and PHY94-20470 at Caltech, the U.S. Department of Energy under Grant No. DE-FG03-87ER40347 at CSUN, and the Institute of Mathematical Sciences at the Chinese University of Hong Kong. M.C. acknowledges the support of a summer research grant and a direct grant (No. 2060105) of the Chinese University of Hong Kong.

-
- [1] E. Shuryak, *Comments Nucl. Part. Phys.* **21**, 235 (1994).
 [2] T. Schäfer and E. V. Shuryak, *Rev. Mod. Phys.* **70**, 323 (1998).
 [3] C. Bernard *et al.*, *Phys. Rev. Lett.* **78**, 598 (1997).
 [4] G. Boyd, F. Karsch, E. Laermann, and M. Oevers, IFUP-TH 40/96 and BI-TP 96/27, hep-lat/9707046, 1996; P. deForcrand, M. G. Pérez, J. E. Hetrick, and I.-O. Stamatescu, *Nucl. Phys. B (Proc. Suppl.)* **63**, 549 (1998).
 [5] Ph. de Forcrand, M. G. Pérez, and I. O. Stamatescu, *Nucl. Phys.* **B499**, 409 (1997).
 [6] I. Montvay and G. Münster, *Quantum Fields on Lattice* (Cambridge University Press, Cambridge, England, 1994), and references therein.
 [7] M. Teper, *Phys. Lett. B* **171**, 81 (1986); J. Hoek, M. Teper, and J. Waterhouse, *Nucl. Phys.* **B288**, 589 (1987).
 [8] T. DeGrand, A. Hasenfratz, and T. G. Kovacs, *Nucl. Phys.* **B505**, 417 (1997).
 [9] M.-C. Chu, J. M. Grandy, S. Huang, and J. W. Negele, *Phys. Rev. D* **49**, 6039 (1994); *Phys. Rev. Lett.* **70**, 255 (1993); M.-C. Chu and S. Huang, *Phys. Rev. D* **45**, 2446 (1992).
 [10] S. Gottlieb *et al.*, *Phys. Rev. D* **47**, 3619 (1993); <http://physics.indiana.edu/~sg/milc.html>
 [11] Y. Kuramashi *et al.*, *Phys. Lett. B* **313**, 425 (1993).
 [12] B. Allés *et al.*, *Phys. Lett. B* **389**, 107 (1996).
 [13] Th. Lippert *et al.*, *Nucl. Phys. B (Proc. Suppl.)* **73**, 521 (1999).
 [14] B. Allés *et al.*, *Phys. Rev. D* **58**, 071503 (1998).
 [15] M.-C. Chu and S. W. Schramm, *Phys. Rev. D* **51**, 4580 (1995).
 [16] E. Shuryak and M. Velkovsky, *Phys. Rev. D* **50**, 3323 (1994).
 [17] R. D. Pisarski and L. G. Yaffe, *Phys. Lett.* **97B**, 110 (1980).
 [18] E. Witten, *Nucl. Phys.* **B156**, 269 (1979); *ibid.* **B159**, 213 (1979).
 [19] B. Harrington and H. Shepard, *Phys. Rev. D* **17**, 2122 (1978); **18**, 2990 (1978); D. J. Gross, R. D. Pisarski, and L. G. Yaffe, *Rev. Mod. Phys.* **53**, 43 (1981).